Full Length Article

The underlying difference of metastatic and non-metastatic breast cancer cells in configuring type I collagen fibres to promote migration by cell mechanics

Mingxing Ouyang [a,*,1], Weihui Chen [a,b,1], Ting Zhou [a], Hongjie Liu [a,b], Lei Liu [a], Bing Bu [a], Linhong Deng [a,**]

[a] *Institute of Biomedical Engineering and Health Sciences, School of Medical and Health Engineering, Changzhou University, Changzhou, 213164 China*
[b] *School of Pharmacy, Changzhou University, Changzhou, 213164 China*

ARTICLE INFO

ABSTRACT

The progression of tumors is heavily influenced by mechanical properties of their microenvironment. In this work, we applied micropatterned models with varying distances and shapes to investigate the differences between metastatic MDA-MB-231 and non-metastatic MCF-7 breast cancer cells in reconfiguring extracellular matrix to promote cell migration induced by cell mechanics. Both cancer cells were able to rearrange type I collagen (COL) to form fibre threads, in which MDA-MB-231 consistently migrated more rapidly than MCF-7, ranging from geometrical square arrays with different spacings to complex polygonal models. MDA-MB-231 displayed higher capability of reorganizing fibre bundles at longer distance (800 μm). Further looking for differences in cell molecular mechanisms, siRNA knockdown inhibiting either integrin β1 or Piezo1 decreased fibre assembly and reduced the difference in COL remodeling and migration between two cancer cells. MDA-MB-231 showed inhibited migration with integrin knockdown, whereas scattering migration with Piezo1 knockdown, indicating cells losing directional mechanosensation. After inhibiting junctional E-cadherin with siRNA, MCF-7 cells migrated faster, resulting in reduced difference in comparison to MDA-MB-231 that didn't express E-cadherin. In summary, this work has explored the biomechanical differences between metastatic and non-metastatic breast cancer cells regarding COL fibre matrix remodeling and cell movements. The significant differences in E-cadherin expression in the two breast cancer cells had an effect on cell migrations. The results of this study provide research approaches for evaluating therapeutic effort on breast cancer.

1. Introduction

The correlation between biomechanics and human diseases has become an increasingly prominent area of scientific research in recent years.[1] Tumors cause the second leading mortality besides cardiovascular diseases. With the advancement of scientific research, people are increasingly recognizing the vital role of the microenvironment in the initiation and progression of malignant tumors. Specifically, these tumors are heavily influenced by the mechanical properties of their immediate microenvironment.[2] The growth and development of a tumor causes changes in the mechanics of its microenvironment, and altered conditions of cellular mechanics can influence cancer development.[3,4] In order to effectively treat cancer, it is necessary to understand the cellular biomechanical conditions that contribute to tumor metastasis and those that inhibit these processes.[5] Therefore, it has become increasingly apparent that tumor biomechanics is a critical aspect of cancer treatment that requires significant attention.

It has been found that cells can sense and signal through mechanical forces, and other cells at great distances also respond to the generated mechanical signals.[6] Cells mechanically sense and respond to other cells at relatively large distances (such as many times of the diameter of the cell) through the extracellular matrix (ECM),[7–9] and then the cells move towards each other.[8] Recently published studies have confirmed that cells can transmit traction through the matrix, thereby realizing distant mechanical communication between cells, resulting in directional cell migration.[10] These studies and discoveries can show that cells far apart can sense each other and respond to biomechanical signals in the environment to achieve mechanical communication.[10,11]

Distant mechanical communication between cells is essential for tissue development and homeostasis.[12,13] Although the processes of mechanical communication between cells via the ECM have been observed,[14] understanding the specific molecular mechanisms involved in distant communication requires more investigation.[13,14] The communication between cells and the extracellular matrix (ECM) plays a crucial role in numerous physiological processes, such as fundamental cellular functions,[12] including migration, proliferation, gene expression and differentiation, cancer metastasis,[15] fibrosis, and wound healing,[16,17] in which cells deform and alter the mechanical structure of the ECM to regulate their contractility and physiological activity.[17] Cells can respond to the distant mechanical action by transferring traction between cells through ECM,[10,18] reconstructing collagen fibers,[11,19] and remodeling the extracellular matrix.[20–22]

The main cause of high cancer mortality is the metastasis of tumor cells,[23,24] which refers to the invasion, spread and colonization of cancer cells from the confines of the original tumor site to other organs and systems.[25,26] Cell-ECM mechanical communication is also an important mediator of cancer progression.[27,28] Metastasis is almost always related to the interaction between cancer cells and ECM.[29] Cancer cells arrange collagen fibers to reshape ECM through various mechanisms,[27,28] including crossing the basement membrane, invading tissue,[29] degrading the matrix, and remodeling the matrix.[27] Therefore, it is by changing the mechanical properties of the microenvironment,[29,30] that aggressive cancer cells form malignant transformations that lead to tumor metastasis.[31,32]

In previous studies, we identified the assembly and remodeling of the ECM as physiologically important events in vivo.[33,34] Cell clusters encapsulated in type I collagen (COL) form dense and aligned fibrillar bundles between them,[35,36] which establish distant communication through matrix-transferred mechanics, giving rise to directional migration and self-assembly of cell groups.[10,36,37] More research is still needed on how cancer cells biomechanically regulate COL assembly over long ranges,[33] especially the difference between normal and malignant cells. Breast cancer is the most common malignant tumor in women worldwide,[38] and research on the biomechanical differences between metastatic MDA-MB-231 and non-metastatic MCF-7 breast cancer cells can help understand the progress of breast cancers. Previous study has reported that MDA-MB-231 cells show more intravasation than MCF-7 in Matrigel, however, the mechanism is to be identifed.[25] Thus, this study attempted to investigate the differences between MDA-MB-231 and MCF-7 in inducing COL fibre matrix remodelling and migration under distant mechanical effects. How cancer cells remodel the ECM was investigated by introducing the fluorescent protein EGFP-CNA35 staining to label the COL,[33] and then using PDMS model arrays in order to substantiate collagen fibre bundles formation and visualization studies.[39] The results showed that there were significant differences in the remodeling of extracellular matrix and cell migration between the two types of cancer cells under distant biomechanics, with non-metastatic cancer cells being more significantly affected by distant mechanics. Plasma membrane-localized integrin and Piezo were crucial in distant mechanosensation of the cancer cells to promote migration. In comparison to MCF-7, deficiency in E-cadherin expression of MDA-MB-231 seemed important in the migration.

2. Materials and methods

2.1. Materials

2.1.1. Cell type and origin

Human breast cancer MDA-MB-231 cell line and MCF-7 cell line, which are breast epithelial cancer cells, of which MDA-MB-231 cells are malignant with high metastasis and invasiveness, and MCF-7 cells are non-metastatic, were purchased from BeiNa Biological Co., LTD.

2.1.2. Main reagents and instruments

DMEM high-glucose medium, RPMI 1640 medium, Opti-MEM medium, fetal bovine serum (FBS), 0.25 % trypsin, transfection kit Lipofectamine 3000™ were purchased from Thermo Fisher Scientific in the United States; the Rat Tail Collagen Type I (type I Collagen, COL) and Neutralization Solution were purchased from Advanced Biomatrix; glass-bottom confocal dish purchased from NEST company; CO2 cell incubator purchased from Japan Sanyo; Live-cell inverted fluorescence microscope (Primo Vert) was purchased from Zeiss, Germany; the micropattern chip containing a film mask and a silicon wafer was purchased from Suzhou MicroFlu Technology Co. and In Situ Co., Ltd.

2.2. Methods

2.2.1. Preparation of PDMS molds

The micro-patterned arrays of cell clusters were prepared according to the method from our previous work.[19,20] We used the software AutoCAD to design the arrays of circle distributions, which circles were set as 200 μm in both diameter and depth. The parameters of the specific models used are shown in Table 1, and the corresponding silicon wafer molds were ordered from local manufacturer. Polydimethylsiloxane (PDMS) base and crosslinking agent (Sylgard 184 kit, Dow Corning) were mixed thoroughly at a mass ratio of 10:1, vacuumed to remove air bubbles and then casted uniformly on silica gel molds, cured at 80 °C for more than 4 h. The elastic replica of the molds was obtained by hardening of the PDMS and further cut into the size required for the experiments, washed with purified water and then soaked in 75 % ethanol to sterilize.

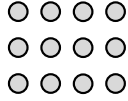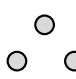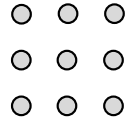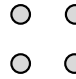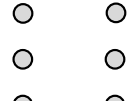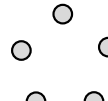#### 2.2.2. EGFP-CNA35 protein purification and quantitative assay

The DNA construct for pET28a-EGFP-CNA35 was purchased from Addgene (cat. no. 61602),[10] and the method for expression and purification of EGFP-CNA35 protein is described specifically in previous work.[40,41] Preparation of EGFP-CNA35 fluorescent protein required steps such as bacterial transformation and expression, and further protein extraction and purification. Firstly, pET28a-EGFP-CNA35 plasmid was transformed into BL21 (DE3) competent bacteria, which was amplified and cultured in LB medium, and then 0.4 mM isopropyl β-ᴅ-1-thiogalactopyranoside (IPTG) was added to induce the protein expression for overnight culture at room temperature. Bacterial pellets were resuspended with B-PER bacterial lysate (Thermo Scientific; cat. no. 78243), and HisPur Ni-NTA agarose resin was added to bind EGFP-CNA35 protein with $6 \times$ His tag, and then the mixture was transferred to a purification column, and the desired protein solution was extracted through the steps of washing, elution, and dialysis. The concentration of purified EGFP-CNA35 protein was measured by BCA protein (Beyotime; cat. no. P0010S) quantification assay.[42] The protein samples were stored as small aliquots at −80 °C.

2.2.3. Cell culture and experimental procedures

MDA-MB-231 cells and MCF-7 cells were cultured in RPMI 1640 medium and high-glucose DMEM medium, respectively, both supplemented with 10 % fetal bovine serum and 1 % penicillin/Streptomycin antibiotics. The cells used in the experiments were generally maintained up to 10 passages.

Table 1
The parameters for various geometric patterns.

Distribution geometries of circles	Geometrical patterns (circles with 200μm in diameter)	Mutual space separation(μm)	Distribution geometries of circles	Geometrical patterns (circles with 200μm in diameter)	Mutual space separation(μm)
Square Arrays		600	Triangle		600(side)
Square Arrays		800	Square		600(side)
Linear		Transverse (2000) Lengthwise (800 or 1000)	Pentagon		600(side)

The 2 % agarose gel solution (20 g/L) was prepared as follows: 2 g of agarose was added into 100 mL of sterile PBS (Phosphate-Buffered Saline), heated and dissolved, then placed in the refrigerator at 4 °C for reserve. The disinfected PDMS molds were prepared in advance. Before starting the experiment, 150 μL of heated 2 % agarose solution was spread evenly on the glass bottom of 35 mm confocal dish, and the PDMS mold was quickly and gently pushed downward on the liquid surface, then cooled down to obtain the desired hole depth of the mold. The cells were washed twice with 1 × PBS, digested with trypsin, and cell counting was performed. 200 μL of similar numbers of MDA-MB-231 and MCF-7 cells ($9.6*10^5$ cells/mL) were inoculated into concave wells on the agarose gel to form our desired cell mass arrangement. The floating cells on the gel surface were gently washed away. Technically, addition of cells on the agarose gel could be repeated if needed.

The type I collagen (Advanced BioMatrix; cat. no. 5153) gel preparation process was carried out on ice. The COL mixture consisted of 1 mg/mL type I collagen solution, Neutralization Solution, 0.2 mg/mL EGFP-CNA35 protein (diluted to 1 mg/mL in advance) and 1xPBS solution on ice. Sequentially, first mixed COL and CNA35-EGFP according to the volume ratio of 5:1 and incubated for 15 min on ice; then added Neutralization Solution (COL: Neutralization Solution = 9:1), and the remaining 1xPBS was added to dilute the COL concentration from the original 4 mg/mL to 1 mg/mL. Afterwards, 400–500 μL of the mixed COL solution was added on the patterned cells-containing agarose gel, and spread by using the pipette tip across the bottom surface of the dish in order to attach the COL hydrogel onto the agarose gel. Then placed the sample in 37 °C cell culture incubator for 15–30 min, the cells would be completely encapsulated in the COL gel, and continued to supplement with 2 mL of the corresponding medium for further culture incubation. Finally, live cell imaging was performed at different time points to check the fluorescent COL fibre assembly and cell migrations.

2.2.4. Live cell microscopy imaging

In the imaging experiments, the Zeiss live-cell inverted epifluorescence microscope (Primo Vert) was used, of which combines high efficiency and outstanding optical performance. During live cell imaging, × 5 and × 10 magnification objective lenses were selected, and the cell samples were placed in an equipped incubation box maintaining 37 °C and 5 % CO2 on the microscope stage. Rapid switching between the FITC and brightfield imaging channels was controlled by the Zeiss software system, thus ensuring that image data from both channels were acquired almost simultaneously. Fluorescence images were acquired every 12h for 36h or 48h during the experimental process. After each imaging experiment, the cell samples were still kept in the regular cell culture incubator.

2.2.5. siRNA transfection with Q-PCR measurements and western blot protein detection

For cell experiments requiring siRNA transfection, cells were inoculated into 6-well plates at ~40 % density one day in advance. On the following day, 5 μL human ITGB1 siRNA (Thermo Fisher Scientific; cat. no. AM16704), Piezo1 siRNA (RiboBio; cat. no. siB151127111307), E-cadherin siRNA (RiboBio; cat. no. siB08716150928), or common control siRNA (50 nM of final concentration in 2 mL of antibiotic-free medium) was transfected into the cells by using Lipofectamine 3000™ (Thermo Fisher Scientific; cat. no. L3000015; 5 μL) reagent. After incubation for about 8 h, changed the medium and waited for 48–72 h for subsequent cell experiments. After E-cadherin siRNA transfection, the decrease of mRNA expression in MCF-7 cells was assessed by real-time quantitative PCR (qPCR), and the experimental manipulation regarding qPCR was described in details in our recent work.[43] The qPCR primer sequences used in the experiments are listed in Table 2.

The Western Blot protein assay was applied to detect the expression of protein levels,[44] and we used it here to validate the protein components that were expressed at different levels in two cancer cells. Firstly, the protein sample extraction was prepared and the cells were counted to select approximately the similar number of MDA-MB-231 versus MCF-7 ($9.2*10^5$ cells each) and added with 100 μL of 2 × SDS-PAGE Sample Loading Buffer (Beyotime; cat. no. P0015B). The cell lysate was boiled at 100 °C for 10 min to obtain protein samples, which can be stored at −20 °C in volume divided quantities. Aliquots (20 μL) of cell protein samples and protein molecular weight markers were loaded into the wells of a 10 % SDS-PAGE gel, and the gel electrophoresis was run at 100 V for 1–2 h. Proteins are transferred from the gel to a PVDF membrane, blocked with 5 % BAS solution, then incubated with E-cadherin primary antibody (Invitrogen; cat. no. PA532178), or internal reference Tubulin antibody (Beyotime; cat. no. AT819; 1:1000) and secondary antibodies. Finally, the PVDF membrane was placed on an infrared laser imager for exposure imaging.

Table 2
The primer sequences of qPCR for measuring E-cadherin mRNA levels.

Gene name	Primer(forward)	Primer(reverse)	Company
E-cadherin	GCTGGACCGAGAGAGTTTCC	CAAAATCCAAGCCCGTGGTG	GENERAL BIOL
GAPDH	GTACGACTCACTATAGGGA	AGGTCCACCACCCTGTTGCTGT	

2.2.6. Collagen fibre and cell area quantification

The quantitative statistics of collagen fibres were performed using ImageJ software. In the procedure, the angle of the image was adjusted so that the collagen fibre appeared in the top-down direction, and then a rectangular frame of appropriate size was drawn so that the collagen lines fell in the middle of the selected region. Using the "plot profile" function in ImageJ, the resulting data representing the average fluorescence intensity (FL) from left to right was copied to Excel and saved. The data acquired for each ROI was fed into Origin 2020 to generate an average fluorescence distribution curve along the selected region. The sum (S_{max}) of 7 points around the maximum intensity value (3 values on the left and 3 values on the right) and the sum (S_{min}) of 7 values on both ends of the curve (3 values on the leftmost and 4 values on the rightmost) were then calculated. The FL ratio was defined as S_{max} divided by S_{min} (FL ratio = S_{max}/S_{min}), and the ratios at the 0, 12, 24, and 36 h time points were generally counted. GraphPad Prism 6.0 was used to statistically compare between the initial time point and later ones. To quantitatively analyze the fluorescence intensity ratio of two cancer cells at the same time, the fluorescence ratio of 12 h or 24 h was normalized compared to the initial state and referred to as the fluorescence intensity change rate. The initial fluorescence distribution is uniform, so the FL ratio is basically about 1.0. With the growth of collagen fibres, fluorescence density changes, and we define the initial fluorescence change rate as 100 %. The Fluorescence intensity change rate is defined as follows:

$$Fluorescence\ intensity\ change\ rate = \left(\frac{FL\ ratio_{12(or\ 24)}}{\overline{X}_0} - 1\right)*100\%$$

where FL ratio$_{12(or\ 24)}$ is the FL ratio of 12 h or 24 h, and $\overline{X}_0$ is the 0 h average of all FL ratios. The quantification procedure for fluorescence COL fibres was demonstrated in Fig. S1(A-C, F-H).

Individual cell cluster areas of bright pictures were counted using ImageJ software. Single clear cell clusters were selected as much as possible and cell clusters area data were obtained by ticking the cell clusters shape using the polygon framing tool. To quantitatively analyze the area change ratio of two cancer cells at the same time, the area of 12 h or 24 h was normalized compared to the initial state and referred to as the area change rate. In the initial state, the cell clusters are in a circular state, and the size of each mold hole is the same, so area of the cell clusters was basically the same at this time, and the initial area change rate was defined as 100 %. The area change rate is defined as follows:

$$Area\ change\ rate = \left(\frac{Area_{12(or\ 24)}}{\overline{y}_0} - 1\right)*100\%$$

where Area$_{12(24)}$ is the cell clusters area of 12 h (24 h), and $\overline{y}_0$ is the 0 h average of all areas. By comparing the changes in the area of cell clusters between the two cancer cells from the initial time to the same time, the speed of cancer cell migration is reflected. The quantification procedures for cell migration areas are shown in Figs. S1(D, E, I, J).

The COL fluorescence curves and graphs of scattering dots were processed by Origin 2020, GraphPad Prism 6, and Excel software; and the cell cluster area graphs of scattering dots were processed by GraphPad Prism 6 software. Student's t-test was applied for statistical analysis between each two groups such as the control or initial group and the experimental group. *, **, ***, **** represent 'p value' < 0.05, 0.01, 0.001, 0.0001 for significant difference respectively, while 'NS' for no significant difference.

3. Results

3.1. Cancer cells reconfigure collagen matrix to promote migration under 600 μm model arrays

Using micro-patterning techniques, we applied PDMS model arrays with 600 or 800 μm spacing apart in this study, which procedures are depicted in Fig. 1A. Through this well-arranged distribution of cell clusters, MDA-MB-231 and MCF-7 were observed to promote fibrillogenesis of the collagen matrix under distant cell mechanical action (Fig. 1). We seeded the same density of both cancer cells into agarose gel wells imprinted with the matrix model, added COL matrix gel homogeneously mixed with EGFP-CNA35, and performed live cell imaging every 12 h for up to 36 h. The results showed that from the initial up to 24 h, both MDA-MB-231 and MCF-7 had formed clear matrix-style collagen fibre bundles (Fig. 1Bb$_1$, Cc$_1$). More details on the progressive fibre growth are shown in the Supporting Information (Figs. S2A and C). The fluorescence quantification (Ratio = S_{max}/S_{min}) and intensity distribution showed a gradual growth trend of the collagen fibres, with ratios ranging from initial 1.0 to 1.1–1.2. The ratio didn't vary much over time after collagen threads had already formed (Fig. 1Bb$_2$, Cc$_2$). More information on the fluorescence timing quantification is provided in the Supporting Information (Figs. S2B and D). We then selected representative 12h and 24h fluorescence change rates (the ratio percentage of fluorescence intensity at 12h or 24h–0h), and found that the change was about 5 % for both types of cancer cells, with the one of MDA-MB-231 slightly higher than MCF-7 at 12h (Fig. 1D).

Since there was little difference in the ability of MDA-MB-231 and MCF-7 to reconstitute the extracellular matrix to form collagen fibre bundles under the distance of 600 μm, we analyzed the differences in terms of changes in their migration areas. It was found that MDA-MB-231 grew gradually from the initial 24,000 μm² to 122,000–135,000 μm² (Fig. 1Bb$_3$) and MCF-7 grew from 17,000 μm² to 43,000–59,000 μm² (Fig. 1Cc$_3$) in the time period from 0 h to 24 h. Then we continued to compare the spreading area rate of the two cells (the percentage change of the area at 12h or 24h–0h), and at 12h the rate of MCF-7 area change was about 120 %, and the rate of MDA-MB-231 was about 400 %, which was more than the MCF-7 by 280 % (Fig. 1E); the rate of MCF-7 was about 200 % and that of MDA-MB-231 was about 450 % at 24h, so the malignant breast cancer cells still increased by 250 % more than the non-metastatic breast cancer cells (Fig. 1E). We analyzed the differences in the migration of the two types of cancer cells by comparing their rates of change in area, and it was clear that MDA-MB-231 migrated more rapidly than MCF-7 at all times.

3.2. Cancer cells reconstitute collagen matrix to promote cell migration in an 800 μm model arrays

Next, we used a matrix model with a spacing gap of 800 μm to observe the formation of collagen lines and the difference in the migration speed of the two cancer cells in reconstructing the extracellular matrix at a longer distance. It was found that MDA-MB-231 (Fig. 2A, left) and MCF-7 (Fig. 2B, left) still formed clear matrix collagen fibres at a separating distance of 800 μm. More details with the gradual fiber growth and fluorescence quantitative statistics were shown in Supporting Information (Figs. S3A and B), and scattering dots with statistical comparison on the FL ratio of the two cells are given in the Supporting Information
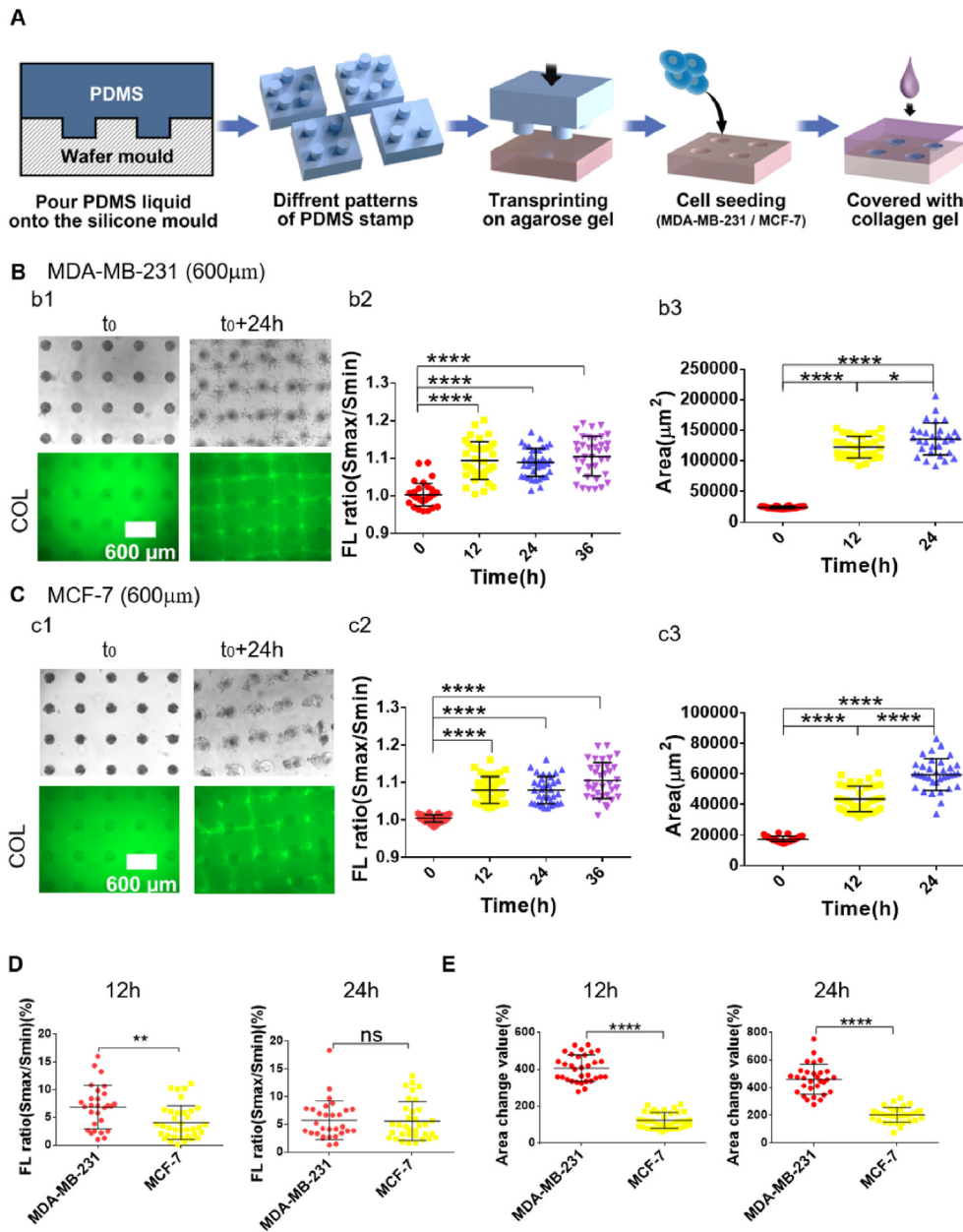
Fig. 1. Differential reconstruction of COL fibres and locomotor migration of cancer cells under distant (600 μm) mechanics. (A) MDA-MB-231 and MCF-7 cell clusters were inoculated in a designed 600 μm matrix array, and the cell clusters were encapsulated with fluorescent COL hydrogel (1 mg/mL), and cell bright field and COL fluorescence images were taken at the indicated times. (B, C) MDA-MB-231 and MCF-7 cell clusters formed clear COL matrix fibre bundles (b_1, c_1); quantification of fluorescence (FL) of COL fibres compared to non-fibre regions based on ratio calibration (S_{max}/S_{min}) (mean ± S.E.M.) (b_2, c_2), each point represents the ratio of a bundle of fibres; quantification of cell clusters area (b_3, c_3), each point represents a cell cluster area at this moment. (D, E) The difference comparisons between MDA-MB-231 and MCF-7 in terms of fluorescence intensity of COL fibres (D) and spreading areas of cell clusters (E) at 12h and 24h. The statistical significance for COL fluorescence and cell clusters area between the initial and indicated time points was evaluated by Student's t-test. *, **, ***, **** represent p value < 0.05, 0.01, 0.001, 0.0001, respectively, whereas 'NS' indicates non-significant differences and so on through the paper.

(Fig. S3C). We compared the 24h fluorescence intensity change rate of the two cancer cells (note: the change rate for the initiation time is normalized to 0). The change rate was about 10.0 % for MDA-MB-231 and 6.5 % for MCF-7 under the distant effect of 800 μm, which were significantly different (Fig. 2C, above). The results on the comparison with the change rate of fluorescence intensity at 12h were shown in the Supporting Information (Fig. S3D, above). Based on the two differential results, it was initially shown that non-metastatic MCF-7 cells might be more affected by the distance between the clusters, and the specific mechanism of the effect needs to be thoroughly investigated.

The following is the analysis of the cell area under the distant action of 800 μm, MDA-MB-231 gradually grows from the initial 19,000 μm² to 58,000–86,000 μm² (Fig. 2A, right), and MCF-7 grows from 18,000 μm² to 29,000–31,000 μm² (Fig. 2B, right). By comparing the 24h area change rate of the two types of cells, it can be obtained that the MCF-7 was about 80 % and MDA-MB-231 was about 340 %, growing 260 % more than MCF-7 (Fig. 2C, bottom). See Supporting Information (Fig. S3D, bottom) for results of the comparison of 12h area change rates.

Then the fluorescence intensity and area of the same cells were compared under different distances of biological force. It was found that at 24h, the fluorescence intensity and area change rate of MCF-7 at 600 μm and 800 μm were different, and 600 μm was about 4.2 % higher than 800 μm in terms of fluorescence density, and 600 μm was about 130 % higher than 800 μm in terms of area change (Fig. 2D). This also confirms that non-metastatic breast cancer cells are more affected by distance, and that the fluorescence intensity is higher and the migration is faster when the two cell clusters are closer to each other. As for MDA-MB-231, the difference in fluorescence density was not significant, and the area change was about 100 % higher at 600 μm than 800 μm (Fig. 2E). The results of the comparisons between 600 μm and 800 μm at 12h showed stronger COL fibre intensity and faster migration at shorter distance for the two types of cells (Figs. S3E and F). Reasonably, at a distance of 600 μm, the two cell clusters are closer to each other and the interaction force is stronger to induce cancer cell migration. Based on the results of the above experiments, there are significant differences between metastatic and non-metastatic breast cancer cells in configuring the COL fibres and
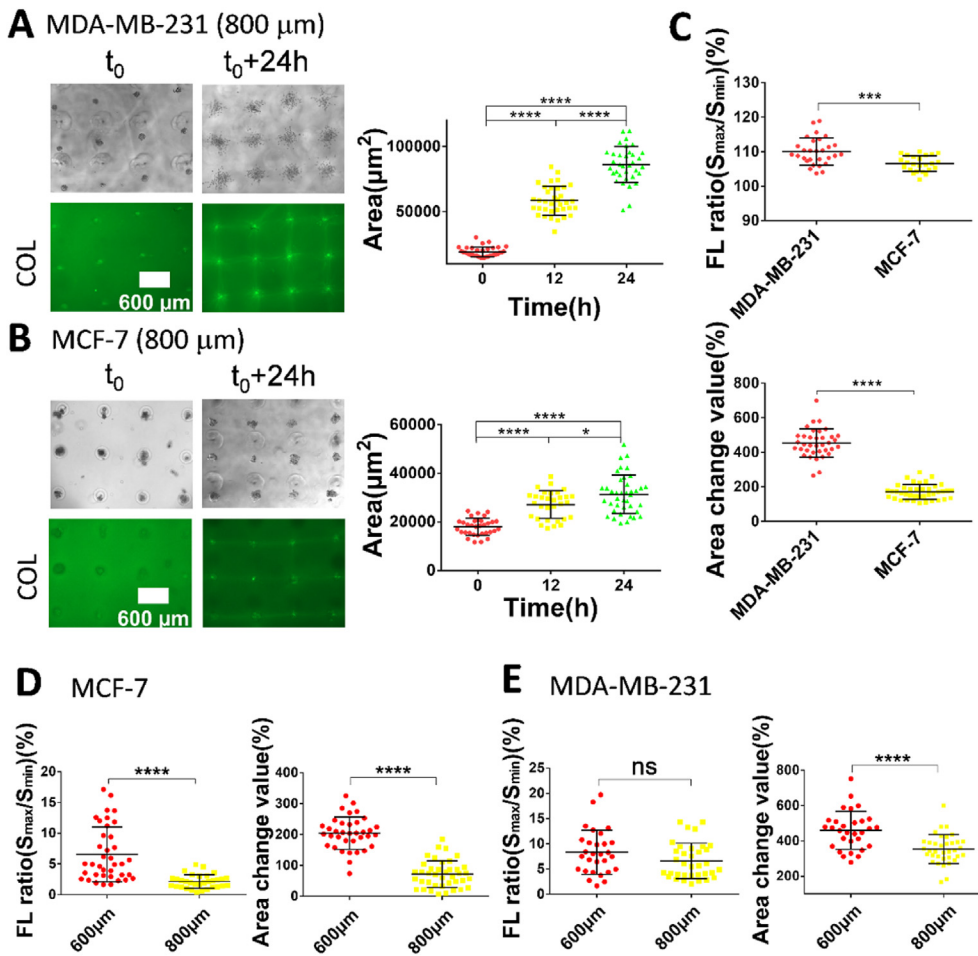
Fig. 2. Cancer cells reconstituted collagen fibre bundles under 800 μm distant mechanics to promote cell migration. (A) Microscopic images of MDA-MB-231 and (B) MCF-7 forming COL matrix fibre strips as well as cell area statistics. (C) Comparison of the rate of fluorescence intensity change between MDA-MB-231 and MCF-7 at 24h with the former being about 7 % higher than the latter, and the former being about 260 % higher than the latter in terms of area. (D, E) Contrast of fluorescence intensity and cell area change rate for (D) MCF-7 and (E) MDA-MB-231 cells at 24h under 600 μm and 800 μm distant effects.

promoting cell migrations, both of which are affected by the distance and MDA-MB-231 cells always migrate faster than MCF-7.

3.3. Differential induction of COL fibre remodeling-promoted migration by cancer cells in linear and separate model conditions

Under the basic matrix models, both cancer cells formed collagen fibres, but the malignant breast cancer cells MDA-MB-231 migrated more rapidly, so we designed a linear model with a longer distance to conveniently observe the cell migration changes. Cell clusters on the line were arranged 800 μm apart, and the lines were at a distance of 2000 μm apart. It was found that MDA-MB-231 and MCF-7 formed collagen fibre bundles along the direction of the line at 800 μm, but not in the direction of 2000 μm (Fig. 3A and B, left). Under the matrix model at 2000 μm further apart, almost no collagen fibres were formed by either MDA-MB-231 or MCF-7 (Fig. 3C and D, left). More details with the gradual fiber growth and fluorescence quantitative statistics were shown in Supporting Information (Figs. S4A and B), and scatter statistics on the FL ratio of the two cells are given in Fig. S4C. Comparing the rate of fluorescence intensity variation at 24h for the two cancer cells, MDA-MB-231 was about 3 % higher than MCF-7 (Fig. 3E, above). The results of the 12h comparisons are shown in Fig. S4E, above.

For the linear model of 800 μm, the area variability of MDA-MB-231 (540 %) was about 400 % higher than that of MCF-7 (130 %) at 24 h, and cells preferred to migrate toward the neighboring clusters (Fig. 3E, right); at a distance of 2000 μm, MDA-MB-231 (520 %) was about 440 % higher than that of MCF-7 (80 %) (Fig. 3F). The results of the 12h comparisons are shown in Fig. S4E&F. It is worth noting that MDA-MB-231 always migrated faster than MCF-7 in all cases.

3.4. Cancer cells induce COL fibre remodeling to promote migration in different geometrical polygons

We further used cell clusters positioned into single polygons including triangles, squares, pentagons, and hexagons (with 600 μm mutual separation between two neighboring clusters and 1000 μm apart between two polygons). Cancer cells reconstructed the extracellular matrix under these model arrays to form corresponding polygonal collagen fibre bundles. When the cell clusters formed individual triangles, strong COL fibres appeared on three sides, and MDA-MB-231 cells migrated toward each other while MCF-7 was less obvious (Fig. 4a$_1$, b$_1$). In single squares, COL fibres were shown up at four sides, and MDA-MB-231 collagen fibres were more clearly defined than MCF-7 (Fig. 4a$_2$, b$_2$). There was also certain fibre growth of MDA-MB-231 samples between two squares which had 1000 μm apart in distance (Fig. 4a$_2$). When the cell clusters were arranged in individual pentagons or hexagons, the COL fibres occurred gradually at the sides to form polygonal shapes, and MDA-MB-231 cells also migrated toward each other along the sides while MCF-7 was less obvious in migration (Fig. 4a$_{3,4}$, b$_{3,4}$). As the cells migrated and moved towards each other, some deformation of the polygonal shapes also occurred.[19] The more details for fibre inductions from single triangles to hexagons and FL ratio as well as cell clusters area statistics are presented in Fig. S5&6, A-D.

By comparing the 24h fluorescence intensity change rates of the two cancer cells in different shapes, it was found that the MDA-MB-231 square had the lowest percentage of change, and the rest of the shapes did not differ much, while the MCF-7 pentagonal and hexagonal had higher change than triangular and square (Fig. 4C and D, left); comparison of the area change ratio of the two cancer cells in different shapes at
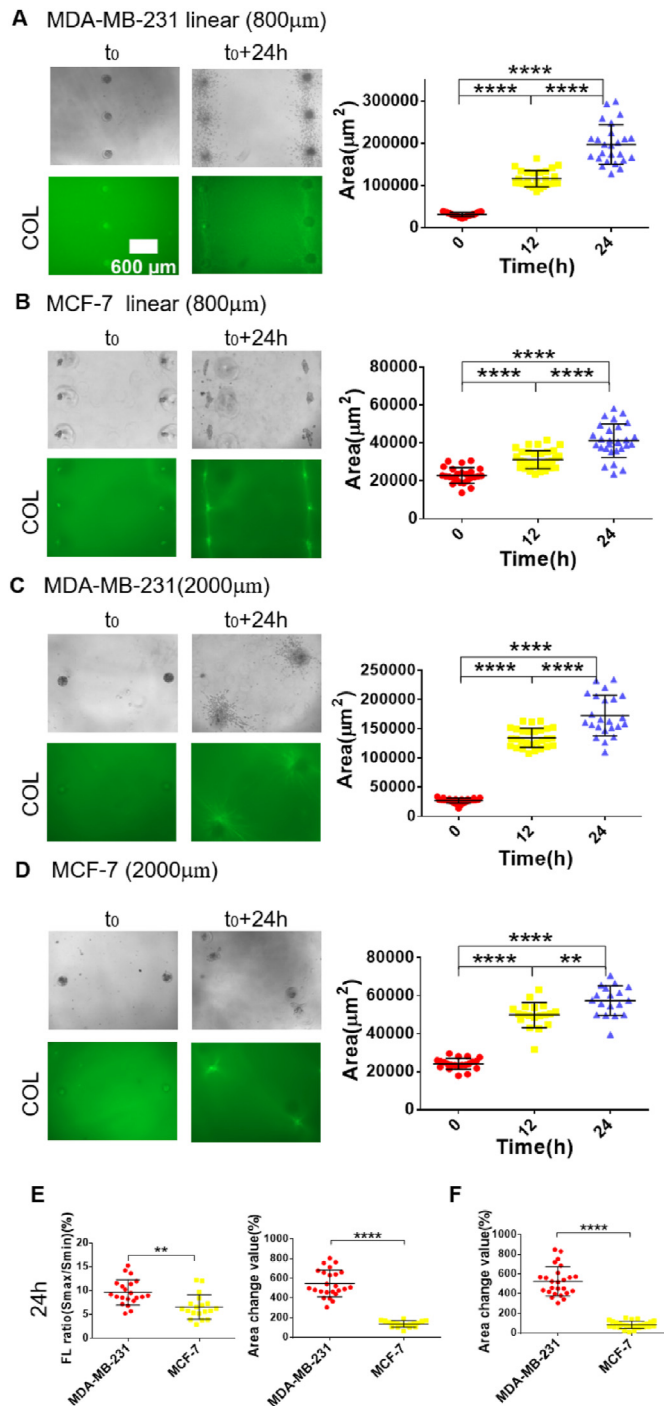
Fig. 3. Differences in cancer cells-induced COL fibre bundling and cell migration at 800 μm and 2000 μm linear models. MDA-MB-231 and MCF-7 cell clusters reconstructed the extracellular matrix to form collagen fibre strips at 800 μm linear model, and increased the distance to 2000 μm, where collagen lines no longer formed. (A, C) Collagen fibre growth images of MDA-MB-231 and (B, D) MCF-7 in the 800 μm linear model and at a distance of 2000 μm, as well as statistical plots of cell area. (E) Comparison of 24h fluorescence intensity change rate between MDA-MB-231 and MCF-7 at 800 μm linear model, where the former is about 3 % higher than the latter; and area change ratio, where the former is about 410 % greater than the latter. (F) The area variability of MDA-MB-231 is about 440 % higher than that of MCF-7 under 2000 μm distant action.

24h shows that the MDA-MB-231 triangle has the highest change ratio, and MCF-7 square has the lowest (Fig. 4C and D, right). MDA-MB-231 migrated faster than MCF-7 in all different polygon models (Fig. 4E).

The results of the 12h comparisons are shown in Fig. S5&6, E. The results of all the above model experiments demonstrated that cancer cells reconfigured COL fibre strips in response to traction forces in the hydrogel, inducing cell migration.

3.5. The importance of integrin β1 and Piezo1 in the induction of COL fibre growth and cell migration

Here, we investigated the roles of two membrane mechanosensitive receptors integrins and Piezo in remote biomechanics as well as cancer cell migration. An 800 μm matrix model was chosen for this study. After downregulation of ITGB1 or Piezo expression with siRNA transfection in cancer cells, COL fibres were slightly inhibited and cell migration was less active in comparison to the control groups (Fig. 5A and B). Fluorescence quantification showed certain inhibition of fibre assembly with integrin β1 or Piezo down-regulation in MDA-MB-231 and MCF-7. When comparing the rates of change in fluorescence at 24h for the two types of cancer cells, it was found that for MDA-MB-231 cells the NC siRNA group was about 5 % higher than both the ITGB1 siRNA group and Piezo1 siRNA group, whereas for MCF-7, the NC siRNA group was about 5–7% higher than both the ITGB1 siRNA group and the Piezo siRNA group (Fig. 5C and D, left). In conclusion, the NC group was higher than the ITGB1 and Piezo siRNA-transfected groups in the rate of fluorescence change. After lowering ITGB1 or Piezo1, the difference in the rate of change in fluorescence at 24h between MDA-MB-231 and MCF-7 was no longer significant (Fig. 5E and F, left), which is contrary to the experimental results in Fig. 3 (Results Section 3.2: without reducing ITGB1 or Piezo1, MDA-MB-231 was approximately 3.5 % higher than MCF-7). These results confirm that the reduction of integrins or Piezo1 had a significant effect on fibre recombination in cancer cells. The more details for fiber inductions as well as cell area statistics under ITGB1 or Piezo1 reduction are presented in Fig. S7&8, A-D.

In terms of area change, the rate of area in the NC group of MDA-MB-231 was about 280 % higher than that of the ITGB1 siRNA group, but not much different from that of the Piezo siRNA group which, however, lost the directional migration and showed scattered migration (Fig. 5A and C, right; quantification of migration distances between two clusters in Piezo group shown in Fig. S8F); the NC group of MCF-7 was about 50 % greater than that of the ITGB1 siRNA group and not much different from that of the Piezo1 siRNA group (Fig. 5D, right). In comparison, integrins had a greater effect on MDA-MB-231 general migration rate, while Piezo1 had a more significant effect on migration direction (Fig. S8F). Next, comparing the area change rate of the two cells showed that MDA-MB-231 was about 70 % higher than MCF-7 after ITGB1 reduction, and MDA-MB-231 was about 300 % higher than MCF-7 after Piezo1 lowering (Fig. 5E and F). These data indicate that ITGB1 lowering decreases the migration rate gap between the two types of cancer cells, whereas Piezo reduction has less impact on migration rates but influencing the migration direction. The results of the 12h comparisons are shown in Figures S7-8, E.

3.6. E-cadherin plays an important role in inhibiting the migration of non-metastatic cancer cells

E-Cadherin has an important role in the metastasis of tumor cells, so we used real-time quantitative PCR (qPCR) to detect the mRNA expression in two kinds of cancer cells and confirmed the previous report that the expression of MCF-7 was much higher than that of MDA-MB-231 (Fig. 6A).[45] Thus, we further conducted Western blot experiments on both cancer cells using E-Cadherin antibody. The results showed that there was a clear E-CAD band in MCF-7 but not in MDA-MB-231 (Fig. 6B), so we approached to investigate whether E-CAD was one responsible factor for the difference in mechanics affecting the two cancer cells. When MCF-7 cells were transfected with E-CAD siRNA, we performed real-time quantitative PCR (qPCR) to detect the decrease of mRNA expression in them, and the decrease in the E-CAD siRNA group was
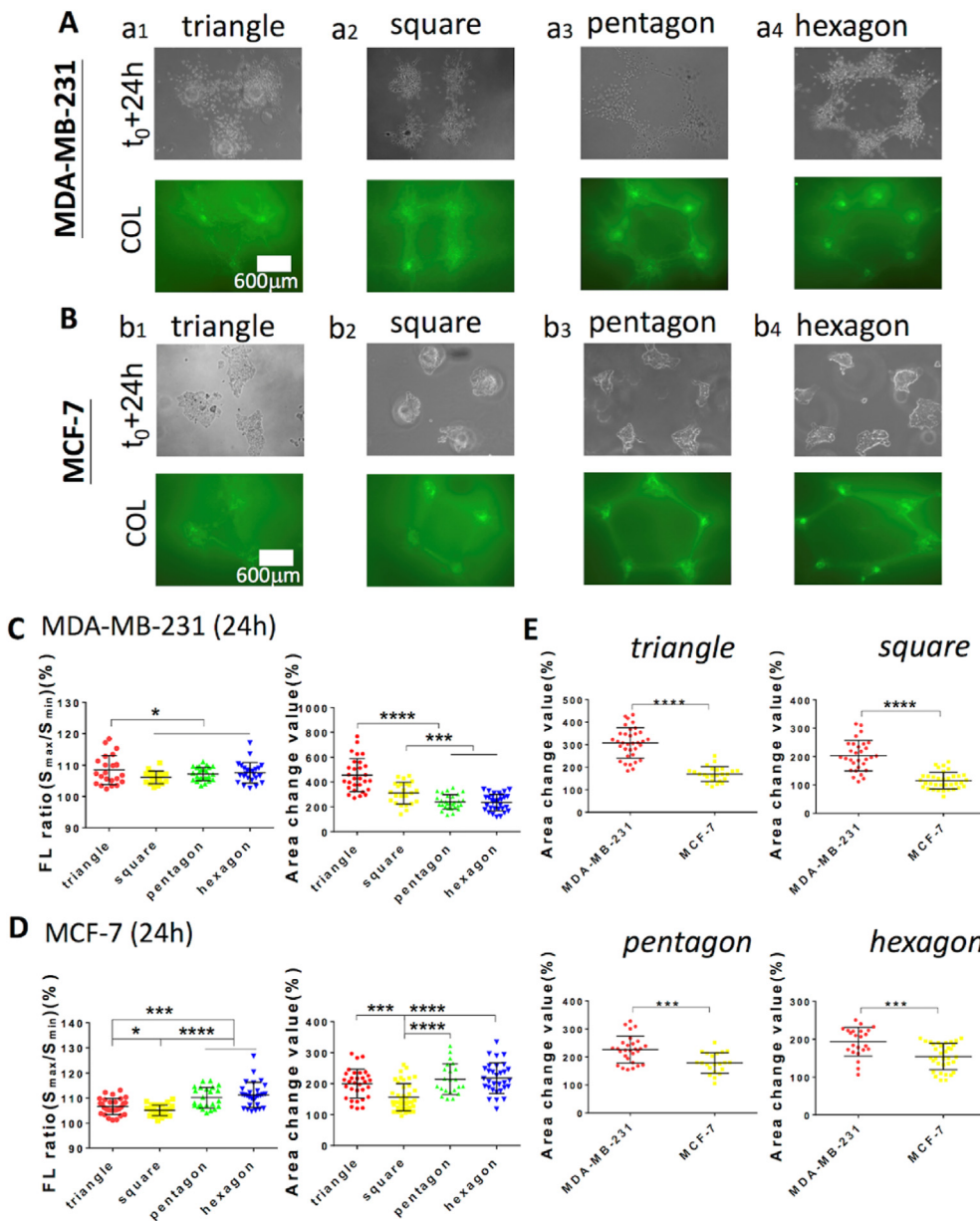
Fig. 4. Comparison of motility migration differences between two cancer cells forming COL fibres with different polygonal shapes. (A, B) MDA-MB-231 and MCF-7 under triangle, square, pentagonal and hexagonal shapes with cell clusters reconfiguring COL fibres to form collagen lines. (C, D) Fluorescence intensity vs. area change rate at 24h between MDA-MB-231 and MCF-7 under different shape models (percentage changes without subtraction of the basal levels). (E) Contrast of 24h area change rate between MDA-MB-231 and MCF-7 under different shape models (percentage changes without subtraction of the basal levels).

about 60 % compared with the NC siRNA and Normal groups (Fig. 6C), which indicated that the E-CAD was effectively reduced in MCF-7. When MCF-7 cells were transfected with E-Cadherin siRNA, collagen bundles were formed in both the experimental and control groups (Fig. 6D and E, left). The cell area spreading increased by more percentage (310 %) in the E-CAD siRNA group than that of NC group (180 %) in 24 h (Fig. 6D and E, right). The more details for fiber inductions and FL ratio are presented in Fig. S9A&B.

Comparison of the rate of change in fluorescence intensity at 24 h between the two groups revealed no significant difference between the NC and E-CAD siRNA group (Fig. 6F, left), which also suggests that E-CAD reduction had less effect on COL fibre growth than ITGB1 and Piezo1 (both of which were about 5 % higher in the NC group than in the experimental group). In terms of the change in area, the NC group was lower than that in the E-CAD siRNA group (Fig. 6F, right), which is contrary to the results of Fig. 5 (Results Section 3.5: the NC group of MCF-7 was about 50 % higher than that of the ITGB1 siRNA group and not much different from that of the Piezo1 siRNA group), suggesting that the reduction of E-CAD promoted MCF-7 cell migration. Based on this

finding, we compared MDA-MB-231 with MCF-7 which reduced E-CAD, and the analysis showed little difference in fluorescence change (Fig. 6G, left). In terms of area change, MDA-MB-231 was about 140 % higher than MCF-7 with reduced E-CAD (Fig. 6G, right), but the area change rate of MDA-MB-231 was about 260 % higher than that of MCF-7 in Fig. 2 (Results Section 3.2.), suggesting that E-Cadherin has resistance to the migration of cancer cells. Without E-Cadherin, migration was faster in MDA-MB-231 cells, and migration in MCF-7 cells with reduced E-CAD were also less different from MDA-MB-231. The results of the 12 h comparisons are shown in Fig. S9C&D. In considering that little E-CAD mRNA and no E-CAD protein expressions were detected in MDA-MB-231 (Fig. 6A and B), these data indicate change of E-Cadherin at the genetic or expression level, which may help promote the metastasis of the breast cancer cells.

4. Discussion

In the human body, cells are surrounded by the extracellular matrix (ECM),[46] and cells are able to communicate mechanically over long
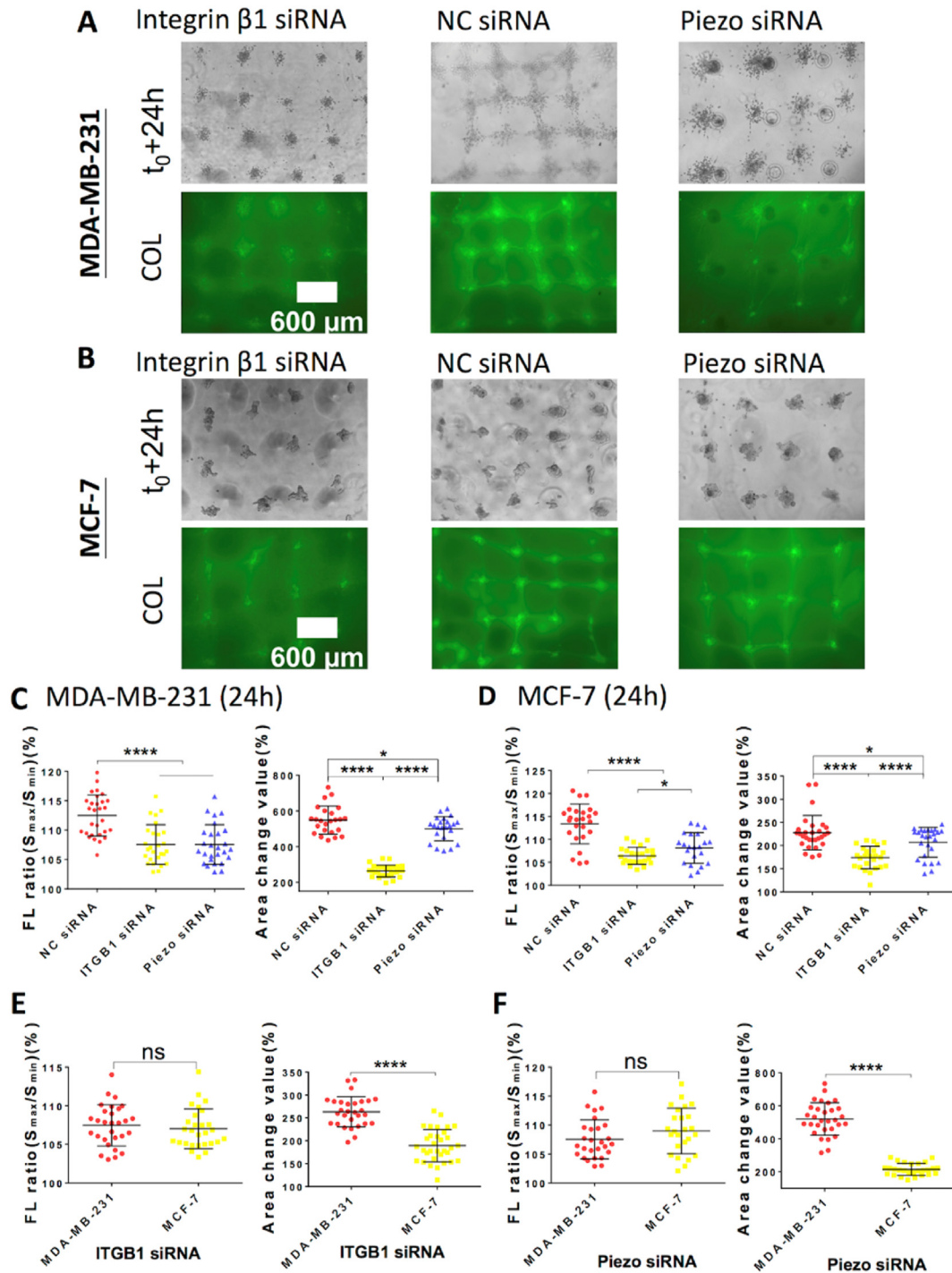
Fig. 5. Effects on cancer cell-induced COL fibre remodeling and cell migration after reduction of Integrin β1 or Piezo1 by siRNA transfection, respectively. (A, B) MDA-MB-231 and MCF-7 remodeled COL fibres to form collagen threads after transfection with ITGB1 or Piezo1 siRNA. (C, D) Comparison of fluorescence intensity and area change rate between NC siRNA transfection and ITGB1 or Piezo1 siRNA transfection groups of MDA-MB-231 and MCF-7 cells. (E, F) Ratio of fluorescence intensity and area change of MDA-MB-231 versus MCF-7 at 24h after transfection of ITGB1 or Piezo1 siRNA. Note: percentage changes without subtraction of the basal levels.

distances[10] by sensing traction forces in the matrix,[11] leading to cell migration. In the present study, we explored the mechanical differences between cancer cells MDA-MB-231 and MCF-7 through both cellular mechanics-induced COL fibre assembly and cell migration.

Significant differences in the induction of matrix remodeling as well as cell migration by two types of cancer cells under distant mechanical effects. Cells can respond to traction forces through the matrix and induce COL remodeling in hydrogels to form cellular lattice

structures. This study explored in more depth the difficult issue of the mechanism of extracellular matrix remodeling for migration of cancer cells at different distances. It was found that both cancer cells could reconfigure COL fibres to form collagen threads under the action of 600 μm and 800 μm long distances (Figs. 1 and 2A, B), however, non-metastatic breast cancer cells MCF-7 were more significantly affected by distance. At 600 μm, there was not much distinction between the two cancer cells in terms of fluorescence rate of change, and a significant
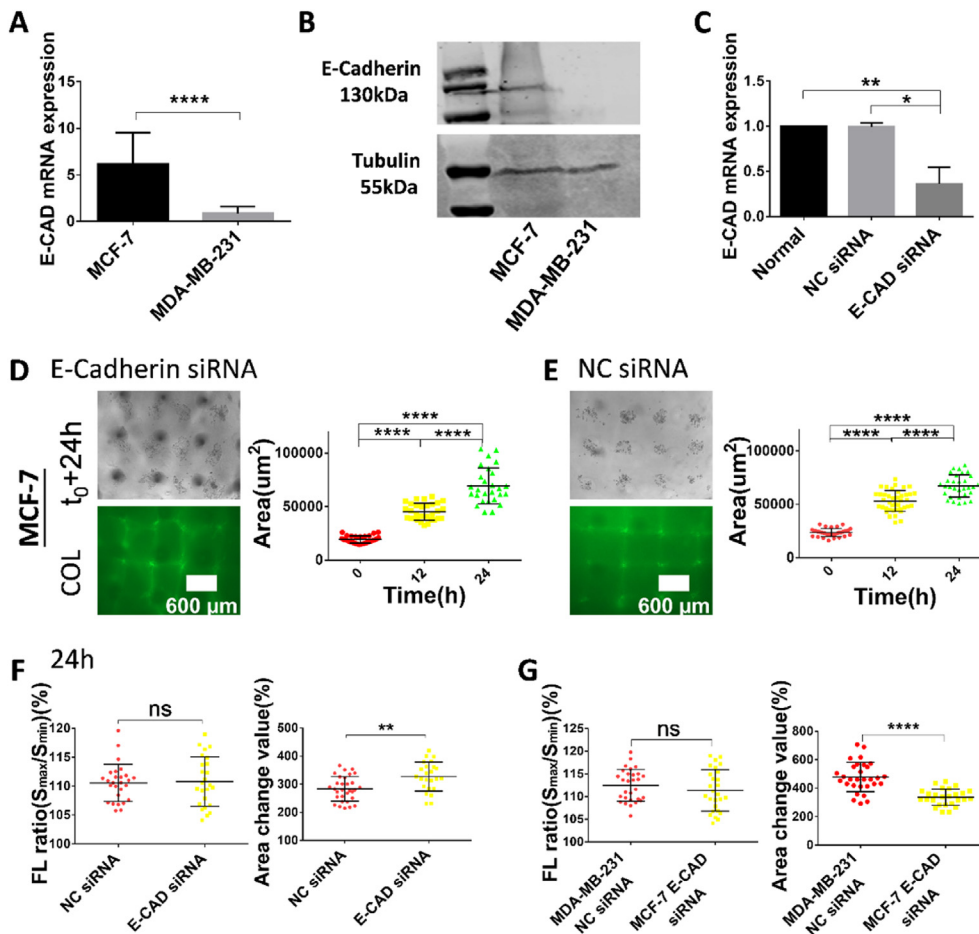
Fig. 6. MCF-7 cells after reduction of E-Cadherin less significantly differed in cell migration compared to MDA-MB-231. (A) Detection of E-CAD mRNA expression in MDA-MB-231 and MCF-7 with qPCR. (B) The E-cadherin protein expression of MDA-MB-231 and MCF-7 detected by Western Blotting with E-CAD antibody. Tubulin bands from the same blotting membrane indicate the sample loading control. (C) The decreased mRNA expression in MCF-7 cells detected by qPCR after transfection with E-CAD siRNA. (D, E) MCF-7 cells transfected with E-CAD siRNA versus control siRNA remodeled COL gel to form collagen bundles, and their cell area statistics. (F) Comparison of fluorescence intensity and area change rate between NC siRNA and E-CAD siRNA transfection groups of MCF-7 cells at 24 h. (G) Comparison of fluorescence intensity and migration rapidity at 24h between MDA-MB-231 as NC siRNA control group and MCF-7 cells transfected with E-CAD siRNA. Note: percentage changes without subtraction of the basal levels.

difference appeared at 800 μm, with clearer and higher fluorescence change rate of MDA-MB-231-induced collagen bundles, which also indicated that the factor of distance had a greater effect on MCF-7. To further explore the effect of distance between cell clusters on reconstituting the extracellular matrix, we again designed a linear model with a lateral direction of 2000 μm and a longitudinal direction of 800 μm, and found that collagen bundles were generated only between cell clusters linearly arranged in the 800 μm direction (Fig. 3A and B). Then we increased the distance to 2000 μm and no collagen bundles were formed in both cancer cells (Fig. 3C and D). These results all indicate that the reorganization of COL fibres induced by different cancer cells is affected by distance, but the MDA-MB-231 cell clusters can still carry out cell-to-cell communication at a much longer distance.

Mechanical communication between cancer cells leads to cancer cell migration, which in turn contributes to cancer progression and tumor metastasis.[27,47] Exploring the mechanisms of cell migration induced by different cancer cells at distant mechanical interactions is a major focus of this study. According to the experimental results, MDA-MB-231 cells showed faster migration changes than MCF-7 regardless of the distance effect (Figs. 1E, 2C and 3E, F). It is noteworthy that the migration pattern common to both cancer cells is that the cell clusters migrate fastest in the arranged 600 μm matrices (Fig. 2D and E, right). At a distance of 600 μm, the two cell clusters are closer to each other and the interaction force is stronger to induce cancer cell migration.

In addition to large-scale arrays, it is also interesting to study the remodeling of single polygonal fibres with different geometries. When inoculated with approximately the same number of both cancer cells in triangular, square, pentagonal and hexagonal arrays of pore depressions, both MDA-MB-231 and MCF-7 cells were able to reconfigure COL fibres to form collagenous threads of the corresponding shapes (Fig. 4A and B).

Among the individual polygons, the square was the most stable[19] and the cancer cell clusters were subjected to more robust distant forces between them, so the square was the lowest in rearranging collagen fibres and cell migration (Fig. 4C and D), but MDA-MB-231 always migrated faster than MCF-7, regardless of the distance model (Fig. 4E).

In this work, the applied method for type I collagen staining with CNA35-EGF was adapted from previous work in which cell contraction-induced alignments of collagen fibers and enhanced rigidity have been characterized by confocal imaging and scanning electron microscopy.[41] Additionally, we observed co-relation between collagen remodeling dynamics and the cell migration rate (Fig. 4C and D), however, the exact relationship between the two parameters hasn't been well identified. For instance, MDA-MB-231 induced similar collagen fibre formation at the distances of 600 μm and 800 μm conditions, but showed faster migration at 600 μm than at 800 μm (Fig. 2E). Our previous work also demonstrated that cell mechanics-induced migration can be independent of collagen fibre assembly.[10] Recent work showed tension force more concentrated spatially at the local regions between two cell clusters, which helps induce collagen fibre assembly and cell migration.[48]

Molecular mechanisms of cancer cells inducing matrix remodeling to promote faster or slower cell migration in response to distant mechanics. Integrin β1 and Piezo are membrane mechanosensitive molecules[43] and integrins play an important role in development and tissue homeostasis;[49] Piezo mediates the proliferation, migration and invasion of cancer cells through a variety of mechanisms.[50] Both play an important role in cellular mechanistic interactions over long distances.[19] Here, we further explored their role in the difference of the two types of cancer cells in inducing COL fibre remodeling to promote cell migration. By reducing ITGB1 or Piezo1 expression with siRNA transfection, both showed reduced COL fibre alignment (Fig. 5C

and D). By comparing the effects of the two membrane mechanosensitive molecules, integrins had a significant effect on both remodeling of the extracellular matrix and cell migration, whereas Piezo1 had a more pronounced effect on migration directions, indicating a role of Piezo1 ion channel in distant mechanosensation between cells. MDA-MB-231 and MCF-7 cells with reduced ITGB1 or Piezo1 no longer differed in inducing remote fibre remodeling, whereas MDA-MB-231 remained faster than MCF-7 in cell migration (Fig. 5E and F).

E-cadherin is a calcineurin found in epithelial cells and the absence of E-CAD is a marker of metastasis of tumor cells.[28,51] So, we started to look at the effect of E-CAD expression difference between the two breast cancer cells. The level of E-CAD mRNA expression in cancer cells was detected by qPCR, and MCF-7 was greatly higher than MDA-MB-231, whereas there was very low E-CAD mRNA expression and no E-cadherin protein expression in MDA-MB-231 (Fig. 6A and B), indicating change of E-cadherin at the genetic or expression level in this metastatic breast cancer cells. Further E-cadherin siRNA transfection of MCF-7 cells did not show much difference between the NC and the experimental group in terms of remodeling collagen fibres, which was the opposite result to ITGB1 or Piezo1 siRNA transfection, whereas E-CAD reduction promoted MCF-7 cell migration (Fig. 6F). The COL remodeling and cell migration speed of MCF-7 cells with reduced E-cadherin were less significantly different from that of MDA-MB-231 (Fig. 6G). Recent work has demonstrated that the collagen fibre assembly is resulted from cell mechanics.[19] MCF-7 cells with E-cad reduction by siRNA didn't change collagen fibre assembly (Fig. 6F), which suggested no remarkable change at the cell mechanics or the induced mechanical property of the matrix hydrogel. Therefore, the difference in E-cadherin expression underlies one mechanism for the two types of cancer cells in promoting cell migration, but not induction of COL fibre remodeling.

5. Conclusions

In this work, we designed PDMS models with varying distances and shapes to investigate the differences between metastatic breast cancer cells MDA-MB-231 and non-metastatic breast cancer cells MCF-7 in reconfiguring the extracellular matrix to promote cell migration induced by distant mechanics, as well as to find out the underlying reasons. Both cancer cells were able to rearrange COL fibres to form a collagen thread, in which MDA-MB-231 showed certain stronger fibre remodeling and consistently migrated more rapidly than MCF-7, ranging from a matrix model with differently arrayed spacings to a complex polygonal model that was independent of each other.

Integrins and Piezo1 mediate distant mechanical communication between cells, as they do for cancer cells, and lowering either protein expression decreased COL fibre bundling and reduced the difference between the two breast cancer cells. Specifically, lowering ITGB1 or Piezo expression inhibits the rate of metastatic cancer cell migration, or causes losing migration direction, respectively. One of the reasons we found for the variability of the two types of breast cancer cells was whether the E-cadherin protein was expressed or not. MCF-7 cells that originally expressed E-CAD showed less significant differences in migration after reduction of this protein compared to MDA-MB-231 that did not express E-CAD. The nearly absence of mRNA and protein expressions of E-cadherin in MDA-MB-231 cells suggests changes at the genetic or expression level in this metastatic breast cancer cells.

In summary, this work aims to explore the differences between malignant MDA-MB-231 and non-metastatic MCF-7 breast cancer cells, particularly in terms of cell migration movements, as cancer cell motility is strongly associated with cancer-related morbidity.[52] We demonstrated the roles of mechanosensitive Integrin and Piezo in COL fibre assembly and cancer cell migration, and that the differences in E-cadherin expression had an effect on cell migration in the two metastatic and non-metastatic breast cancer cells. Inhibiting and blocking the migratory movement of breast cancer cells to reduce or eliminate metastatic spread is likely to be an effective therapeutic strategy for the treatment of

metastatic high-risk cancers.[52–54] The results of this study provide new research approaches for therapeutic advances in breast cancer.

CRediT authorship contribution statement

Mingxing Ouyang: Writing – review & editing, Writing – original draft, Validation, Supervision, Resources, Project administration, Methodology, Investigation, Funding acquisition, Data curation, Conceptualization. **Weihui Chen:** Writing – original draft, Visualization, Methodology, Investigation, Formal analysis, Data curation. **Ting Zhou:** Writing – original draft, Validation, Supervision. **Hongjie Liu:** Formal analysis. **Lei Liu:** Resources, Project administration. **Bing Bu:** Supervision, Methodology, Funding acquisition. **Linhong Deng:** Writing – review & editing, Resources, Project administration, Funding acquisition, Conceptualization.

Ethical approval

This study does not contain any studies with human or animal subjects performed by any of the authors.

Declaration of competing interest

The authors declare the following financial interests/personal relationships which may be considered as potential competing interests as the same:

Mingxing Ouyang reports financial support was provided by National Natural Science Foundation of China. Linhong Deng reports financial support was provided by National Natural Science Foundation of China. Bing Bu reports financial support was provided by National Natural Science Foundation of China. Mingxing Ouyang reports financial support was provided by Jiangsu Education Department. Mingxing Ouyang has patent #CN202311741705.4一种恶性和良性乳腺癌细胞力学差异性的比对方法 issued to Changzhou University. Weihui Chen has patent #CN202311741705.4一种恶性和良性乳腺癌细胞力学差异性的比对方法 issued to Changzhou University. If there are other authors, they declare that they have no known competing financial interests or personal relationships that could have appeared to influence the work reported in this paper.

Appendix A. Supplementary data

Supplementary data to this article can be found online at https://doi.org/10.1016/j.mbm.2025.100113.

References

1. Suresh S. Biomechanics and biophysics of cancer cells. *Acta Biomater.* 2007;3(4): 413–438. https://doi.org/10.1016/j.actbio.2007.04.002.
2. Shen Y, Wang X, Lu J, et al. Reduction of liver metastasis stiffness improves response to bevacizumab in metastatic colorectal cancer. *Cancer Cell.* 2020;37(6):800–817 e7. https://doi.org/10.1016/j.ccell.2020.05.005.
3. Mierke CT. Physical break-down of the classical view on cancer cell invasion and metastasis. *Eur J Cell Biol.* 2013;92(3):89–104. https://doi.org/10.1016/j.ejcb.2012.12.002.
4. Chen X, Tang K, Li X, et al. Biomechanics of cancer stem cells. *Essays Biochem.* 2022; 66(4):359–369. https://doi.org/10.1042/EBC20220014.

5. Ghosh D, Dawson MR. Microenvironment influences cancer cell mechanics from tumor growth to metastasis. *Adv Exp Med Biol.* 2018;1092:69–90. https://doi.org/10.1007/978-3-319-95294-9_5, 0065-2598 (Print).

6. Wang H, Abhilash AS, Chen CS, Wells RG, Shenoy VB. Long-range force transmission in fibrous matrices enabled by tension-driven alignment of fibers. *Biophysical J.* 2014;107(11):2592–2603. https://doi.org/10.1016/j.bpj.2014.09.044.

7. Ma X, Schickel ME, Stevenson MD, et al. Fibers in the extracellular matrix enable long-range stress transmission between cells. *Biophysical J.* 2013;104(7):1410–1418. https://doi.org/10.1016/j.bpj.2013.02.017.

8. Alisafaei F, Chen X, Leahy T, Janmey PA, Shenoy VB. Long-range mechanical signaling in biological systems. *Soft Matter.* 2021;17(2):241–253. https://doi.org/10.1039/d0sm01442g.

9. Cohen O, Safran SA. Elastic interactions synchronize beating in cardiomyocytes. *Soft Matter.* 2016;12(28):6088–6095. https://doi.org/10.1039/c6sm00351f.

10. Ouyang M, Qian Z, Bu B, et al. Sensing traction force on the matrix induces cell-cell distant mechanical communications for self-assembly. *ACS Biomater Sci Eng.* 2020;6(10):5833–5848. https://doi.org/10.1021/acsbiomaterials.0c01035.

11. Ouyang M, Zhu Y, Wang J, et al. Mechanical communication-associated cell directional migration and branching connections mediated by calcium channels, integrin beta 1, and N-cadherin. *Front Cell Dev Biol.* 2022;10:942058. https://doi.org/10.3389/fcell.2022.942058.

12. Li X, Balagam R, He TF, Lee PP, Igoshin OA, Levine H. On the mechanism of long-range orientational order of fibroblasts. *Proc Natl Acad Sci USA.* 2017;114(34):8974–8979. https://doi.org/10.1073/pnas.1707210114.

13. Sapir L, Tzlil S. Talking over the extracellular matrix: how do cells communicate mechanically? *Semin Cell Dev Biol.* 2017;71:99–105. https://doi.org/10.1016/j.semcdb.2017.06.010.

14. Kubow KE, Vukmirovic R, Zhe L, et al. Mechanical forces regulate the interactions of fibronectin and collagen I in extracellular matrix. *Nat Commun.* 2015;6:8026. https://doi.org/10.1038/ncomms9026.

15. Cukierman E, Bassi DE. Physico-mechanical aspects of extracellular matrix influences on tumorigenic behaviors. *Semin Cancer Biol.* 2010;20(3):139–145. https://doi.org/10.1016/j.semcancer.2010.04.004.

16. Chang HY, Sneddon JB, Alizadeh AA, et al. Gene expression signature of fibroblast serum response predicts human cancer progression: similarities between tumors and wounds. *PLoS Biol.* 2004;2(2):E7. https://doi.org/10.1371/journal.pbio.0020007.

17. Abhilash AS, Baker BM, Trappmann B, Chen CS, Shenoy VB. Remodeling of fibrous extracellular matrices by contractile cells: predictions from discrete fiber network simulations. *Biophysical J.* 2014;107(8):1829–1840. https://doi.org/10.1016/j.bpj.2014.08.029.

18. Xu XP, Safran SA. Nonlinearities of biopolymer gels increase the range of force transmission. *Phys Rev E.* 2015;92(3). ARTN 03272810.1103/PhysRevE.92.032728.

19. Ouyang M, Hu Y, Chen W, et al. Cell dynamic mechanics regulates large-spatial isotropic matrix modeling with computational simulations. *Research.* 2023;6:15. https://doi.org/10.34133/research.0270, 0270.

20. Guo CL, Ouyang M, Yu JY, Maslov J, Price A, Shen CY. Long-range mechanical force enables self-assembly of epithelial tubular patterns. *Proc Natl Acad Sci USA.* 2012;109(15):5576–5582. https://doi.org/10.1073/pnas.1114781109.

21. Spatarelu CP, Zhang H, Trung Nguyen D, et al. Biomechanics of collective cell migration in cancer progression: experimental and computational methods. *ACS Biomater Sci Eng.* 2019;5(8):3766–3787. https://doi.org/10.1021/acsbiomaterials.8b01428.

22. Harris AK, Stopak D, Wild P. Fibroblast traction as a mechanism for collagen morphogenesis. *Nature.* 1981;290(5803):249–251.

23. Gensbittel V, Krater M, Harlepp S, Busnelli I, Guck J, Goetz JG. Mechanical adaptability of tumor cells in metastasis. *Dev Cell.* 2021;56(2):164–179. https://doi.org/10.1016/j.devcel.2020.10.011.

24. Kashani AS, Packirisamy M. Cancer cells optimize elasticity for efficient migration. *R Soc Open Sci.* 2020;7(10):200747. https://doi.org/10.1098/rsos.200747.

25. Han W, Chen S, Yuan W, et al. Oriented collagen fibers direct tumor cell intravasation. *Proc Natl Acad Sci USA.* 2016;113(40):11208–11213. https://doi.org/10.1073/pnas.1610347113.

26. Zhang XH. Why cancer cells metastasize? *Med Hypotheses.* 2013;80(5):669–671. https://doi.org/10.1016/j.mehy.2013.01.022.

27. Schwager SC, Taufalele PV, Reinhart-King CA. Cell-cell mechanical communication in cancer. *Cell Mol Bioeng.* 2019;12(1):1–14. https://doi.org/10.1007/s12195-018-00564-x.

28. Labernadie A, Kato T, Brugues A, et al. A mechanically active heterotypic E-cadherin/N-cadherin adhesion enables fibroblasts to drive cancer cell invasion. *Nat Cell Biol.* 2017;19(3):224–237. https://doi.org/10.1038/ncb3478.

29. Mierke CT. The matrix environmental and cell mechanical properties regulate cell migration and contribute to the invasive phenotype of cancer cells. *Rep Prog Phys.* 2019;82(6):064602. https://doi.org/10.1088/1361-6633/ab1628.

30. Erdogan B, Ao M, White LM, et al. Cancer-associated fibroblasts promote directional cancer cell migration by aligning fibronectin. *J Cell Biol.* 2017;216(11):3799–3816. https://doi.org/10.1083/jcb.201704053.

31. Kai F, Drain AP, Weaver VM. The extracellular matrix modulates the metastatic journey. *Dev Cell.* 2019;49(3):332–346. https://doi.org/10.1016/j.devcel.2019.03.026.

32. Zanotelli MR, Zhang J, Reinhart-King CA. Mechanoresponsive metabolism in cancer cell migration and metastasis. *Cell Metab.* 2021;33(7):1307–1321. https://doi.org/10.1016/j.cmet.2021.04.002.

33. Wang J, Guo J, Che B, Ouyang M, Deng L. Cell motion-coordinated fibrillar assembly of soluble collagen I to promote MDCK cell branching formation. *Biochem Biophys Res Commun.* 2020;524(2):317–324. https://doi.org/10.1016/j.bbrc.2020.01.019.

34. Rozario T, DeSimone DW. The extracellular matrix in development and morphogenesis: a dynamic view. *Dev Biol.* 2010;341(1):126–140. https://doi.org/10.1016/j.ydbio.2009.10.026.

35. Sawhney RK, Howard J. Slow local movements of collagen fibers by fibroblasts drive the rapid global self-organization of collagen gels. *J Cell Biol.* 2002;157(6):1083–1091. https://doi.org/10.1083/jcb.200203069.

36. Sopher RS, Tokash H, Natan S, et al. Nonlinear elasticity of the ECM fibers facilitates efficient intercellular communication. *Biophysical J.* 2018;115(7):1357–1370. https://doi.org/10.1016/j.bpj.2018.07.036.

37. Reinhart-King CA, Dembo M, Hammer DA. Cell-cell mechanical communication through compliant substrates. *Biophysical J.* 2008;95(12):6044–6051. https://doi.org/10.1529/biophysj.107.127662.

38. Park M, Kim D, Ko S, Kim A, Mo K, Yoon H. Breast cancer metastasis: mechanisms and therapeutic implications. *Int J Mol Sci.* 2022;23(12). https://doi.org/10.3390/ijms23126806.

39. Lin L, Chung CK. PDMS microfabrication and design for microfluidics and sustainable energy application: review. *Micromachines (Basel).* 2021;12(11). https://doi.org/10.3390/mi12111350.

40. Ouyang M, Lu S, Wang Y. Genetically encoded fluorescent biosensors for live-cell imaging of MT1-MMP protease activity. *Methods Mol Biol.* 2014;1071:163–174. https://doi.org/10.1007/978-1-62703-622-1_13.

41. Shi QM, Ghosh R. Rapid disorganization of mammary acini driven by long-range mechanical interaction. *Biophysical J.* 2014;106(2):174a. https://doi.org/10.1016/j.bpj.2013.11.987, 174a.

42. Cortés-Ríos J, Zárate AM, Figueroa JD, et al. Protein quantification by bicinchoninic acid (BCA) assay follows complex kinetics and can be performed at short incubation times. *Anal Biochem.* 2020;608. https://doi.org/10.1016/j.ab.2020.113904, 1096-0309 (Electronic)).

43. Fang X, Ni K, Guo J, et al. FRET visualization of cyclic stretch-activated ERK via calcium channels mechanosensation while not integrin beta 1 in airway smooth muscle cells. *Front Cell Dev Biol.* 2022;10:847852. https://doi.org/10.3389/fcell.2022.847852.

44. Kurien BT, Scofield RH. *Western Blotting: An Introduction.* Western Blotting; 2015:17–30. chap (Chapter 5). Methods in Molecular Biology.

45. Zhao W, Kuai XW, Zhou XY, et al. Trop 2 is a potential biomarker for the promotion of EMT in human breast cancer. *Oncol Rep.* 2018;40(2):759–766. https://doi.org/10.3892/or.2018.6496.

46. Ouyang M, Yu JY, Chen Y, Deng L, Guo CL. Cell-extracellular matrix interactions in the fluidic phase direct the topology and polarity of self-organized epithelial structures. *Cell Prolif.* 2021;54(4):e13014. https://doi.org/10.1111/cpr.13014.

47. Lintz M, Munoz A, Reinhart-King CA. The mechanics of single cell and collective migration of tumor cells. *J Biomech Eng.* 2017;139(2):210051–210059. https://doi.org/10.1115/1.4035121.

48. Yang C, Wang XC, Xie RP, et al. Dynamically reconstructed collagen fibers for transmitting mechanical signals to assist macrophages tracing breast cancer cells. *Adv Funct Mater.* 2023;33(9). https://doi.org/10.1002/adfm.202211807.

49. Sun Z, Guo SS, Fassler R. Integrin-mediated mechanotransduction. *J Cell Biol.* 2016;215(4):445–456. https://doi.org/10.1083/jcb.201609037.

50. Yu JL, Liao HY. Piezo-type mechanosensitive ion channel component 1 (Piezo 1) in human cancer. *Biomed Pharmacother.* 2021;140:111692. https://doi.org/10.1016/j.biopha.2021.111692.

51. Liu Z, Liu Z, Zhang X, Xue P, Zhang H. RY10-4 suppressed metastasis of MDA-MB-231 by stabilizing ECM and E-cadherin. *Biomed Pharmacother.* 2014;68(4):439–445. https://doi.org/10.1016/j.biopha.2014.03.003.

52. Stoletov K, Beatty PH, Lewis JD. Novel therapeutic targets for cancer metastasis. *Expert Rev Anticancer Ther.* 2020;20(2):97–109. https://doi.org/10.1080/14737140.2020.1718496.

53. Obenauf AC, Massague J. Surviving at a distance: organ-specific metastasis. *Trends Cancer.* 2015;1(1):76–91. https://doi.org/10.1016/j.trecan.2015.07.009.

54. Palmer TD, Martinez CH, Vasquez C, et al. Integrin-free tetraspanin CD151 can inhibit tumor cell motility upon clustering and is a clinical indicator of prostate cancer progression. *Cancer Res.* 2014;74(1):173–187. https://doi.org/10.1158/0008-5472.CAN-13-0275.